Chapter-3

3 Tuning Self-assembled Phases of Bovine Serum Albumin via Hydrothermal Process to Synthesize Novel Functional Hydrogel for Skin Protection against UVB

3.1 Introduction

Skin, the largest organ in the body, has a surface area of about 1.8 m^2 and occupies 16% of the total body mass of an adult[138]. The primary and most important function of the skin in mammals is to provide a protective barrier against various infections caused by fungi, bacteria, UV radiation, and other environmental factors [139]. One of the major reasons for skin cancer is exposure to UV radiation (UV) which is classified as UVA (320-420nm), UVB (290nm-320nm), and UVC (200-290nm). Almost all three, UVC and a part of UVB wavelength, get absorbed by the ozone layer and limit their reach to the earth's surface[140,141]. Ultraviolet rays - B (UVB) can efficiently be absorbed by the cellular molecules of skin, inducing damage within skin cells and a significant cause of melanoma cancer. Several recent studies have reported adverse effects of traditionally used organic and inorganic material-based sunscreens and UVB-blockers. UVA has a minor impact on the skin; however, UVB is the primary threat to human health and is responsible for skin cancer, photoaging, immune suppression, and sunburns[142,143].

Cancer is the most challenging disease to treat and the second most cause of mortality globally. In recent years, there has been a tremendous increase in skin cancer worldwide[144,145]. The major types of skin cancers are basal cell carcinoma, squamous cell carcinoma, Markel cell cancer, and melanoma. In these cancers, melanoma is most

dangerous because of its ability to spread faster to other organs if it is not diagnosed at an early stage and even becomes deadly[146,147]. Therefore, treating melanoma skin cancer is a big challenge. Emerging functional materials give a possible route to treat melanoma by enhancing drug uptake in cancer cells, minimizing toxicity, increasing the circulation time in tumor tissue, etc.

Avoiding excessive solar exposure and using sunscreens comprised of nanoparticles like zinc oxide NPs, etc., are recommended to prevent exposure to UV radiation[148–150]. Currently, the most commonly used sunscreens are based on nano-sized TiO_2 and ZnO nanoparticles[151,152]. Skin exposure to nano-sized particles containing sunscreens leads to the incorporation of inorganic material in the stratum corneum, which can alter the attenuation properties due to particle-particle, particle-skin, and skin-particle-light physicochemical interaction[118,153]. Photocatalytic effects, nanoparticle stabilization after chronic exposure, and free radical production are other major concerns for using these materials as sun blockers. The current scenario demands a new alternative material for skincare treatments, which can be more efficient, and biocompatible, minimizing the side effects and reducing the treatment cost significantly for the patients[149,154–156]. In this regard, functional biomaterials could be an excellent alternative to the nano-sized inorganic nanoparticle to prevent sunburns and skin cancer.

Proteins are biomolecules in nature; thus, they are safe and biocompatible except some toxic proteins. In recent studies, materials scientists have extensively utilized proteins to design novel materials with unique functionality, which further improves their practical applicability[157–160]. The complex structure of proteins is maintained due to various interactions such as electrostatic, van der Waals, hydrophobic, and cation-pi. These molecular interactions give tremendous opportunities to tune them into self-assembled

hierarchal structures. Another fascinating aspect of self-assembled protein materials is hydrogel formation, which has multifunctional properties[161–164]. Protein-based hydrogels are a promising material for various biomedical applications because of their hydrophilic networks, controllable self-assembly, and biocompatibility. Bovine serum albumin (BSA) is a cost-effective, readily and widely available protein. Its primary structure contains a single polypeptide chain of 583 amino acids with a molar mass of 66.4 kDa. BSA is a water-soluble protein with 76% sequence homology and identical pH-dependent conformation with human serum albumin[165,166]. Studies show that BSA has been conjugated with many organic and inorganic compounds to synthesize bio-nanoconjugates, monolayers, and nanoparticles and holds promising applications in the biomedical field[106,167–170].

In this study, BSA has been used as a precursor to synthesize temperature and pressure-dependent phase transition from sol (globular aggregates) - gel (hydrogels) - sol (carbon quantum dots) using a single-step hydrothermal method with the objective to develop an efficient and effective UVB blocker. The synthesized hydrogels exhibit UV - attenuation, self-fluorescence, and high biocompatibility properties that make them suitable for UV-blocker or sunscreen material. BSA has been used as a precursor to synthesize different self-assembled morphologies. Different phases of BSA protein have been synthesized by varying the hydrothermal temperature from 25 ^{0}C to 120 ^{0}C. First sol to gel transition occurs at 70 ^{0}C, where BSA protein transforms into a self-assembled hydrogel phase.

Further heating of BSA protein at 120^{0}C leads to the second phase transition from gel to carbon quantum dots. Developed phases were thoroughly characterized using various physical and optical techniques like SEM, TEM, FTIR, SAXS, etc., to study their efficient applicability in the biomedical field. The biological efficacy of the hydrogels was studied through cytotoxicity studies. Also, UVB blocking efficiency of developed hydrogel in

primary mice skin cell culture as well as *in vivo* in mice model were investigated. *In vivo* study on mice further demonstrated prominent thickening of stratum corneum and epidermis with perivascular edema in the dermis after 5 days of UVB exposure. Hence, this suggests that hydrogel could be a potential candidate for protecting skin from UVB exposure and reducing the threat of skin cancer.

3.2 Results and Discussion

3.2.1 Sol-Gel-Sol Transformations of BSA hydrogel

BSA gels were prepared at different hydrothermal temperatures varying from 25 ^{0}C to 120 ^{0}C with the 40 mg/ml protein concentration without using any cross-linker or chemical agent. At 25 ^{0}C, the BSA solution does not go for the gelation process even after 15 h of heating, and the resultant has the same sol phase as the BSA initial solution. Further heating at 60^{0}C increases the turbidity of the solution but does not initiate the gelation process. One of the plausible reasons is that below the melting temperature (63 ^{0}C), protein starts to unfold and thermal energy and electrostatic forces between the amino acid start to encounter each other during the hydrothermal process [171]. The melting temperature of the BSA is above 63 ^{0}C, so the BSA solution was heated at 70 ^{0}C hydrothermally for 15 h. Heating protein solution at a temperature of 70 ^{0}C changed the turbid sol phase into a very fine gel, and this gel phase remains till the temperature of 100 ^{0}C.

Further heating of the protein solution above 110 ^{0}C leads to new phases, and the phase separation between sol and gel was observed. A significant portion of the protein solution changes into a brownish gel. When the protein solution was heated at 120 ^{0}C, the complete

protein solution was converted into a sol phase and showed the physical and optical properties of carbon quantum dots. All the phases of the BSA are shown in Figure 3.1.

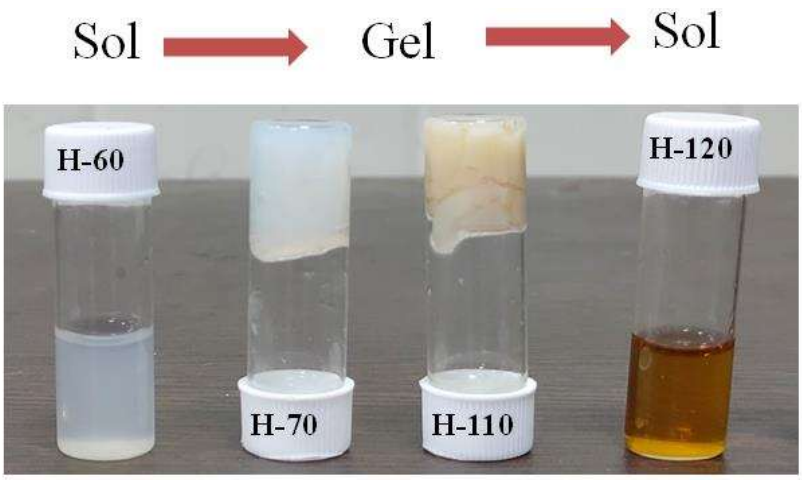

Figure 3.1 Different phases of developed BSA hydrogel at different temperature

The sol-gel-sol phase transition as a function of temperature was tested using the tube inversion method. Thermally elevated phases of BSA showed a significant sol to gel transition at 70^0C and gel to sol transformation at 120^0C. The melting temperature of BSA is 63 ^{0}C, and studies show that BSA has different oligomeric states above and below its melting temperature [172]. The heating of proteins above melting temperature weakens the hydrogen bonds and strengthens the hydrophobic interaction, which alters the diffusion, accessibility and exposure of polypeptide chains segment and dilutes the ligand binding properties[173]. Interactions between electrostatic and hydrophobic interaction connect the protein molecules and lead to the form gel-like structure. The aggregation of BSA can be elevated with temperature, pH, ionic strength, and other external stimuli. These factors play a significant role in protein thermodynamics and can alter the transition temperature of the various phases. As we heated the protein solution at a higher temperature, the strength of

the gel decreased, which was further supported by rheological studies and a tube inversion test. At high temperatures, interactions between the gels start to break, and gel to sol phase transition happens. Physical and optical characterizations of the sol phase confirm the nanostructure of the carbon quantum dots, which are homogeneously dispersed in the medium. Thus, different phases of BSA hydrogels have been synthesized using a single hydrothermal technique by varying temperatures without adding a cross-linker molecule.

3.2.2 Optical characterization of various phases of BSA hydrogels

It was observed that all the BSA hydrogels synthesized at various temperatures show different colors in appearance. As the heating temperature increases, the color of the solutions starts to change, and it becomes a transparent solution to translucent white in the gel phase and dense yellow in the CQDs phase. UV-Vis spectroscopy was used to analyze the optical changes shown in Figure 3.2. UV-Vis spectra of H-25 (hydrogel synthesized at 25 ^{0}C) show BSA's typical characteristic peak observed at 278 nm. As there is an increase in the temperature, protein starts to aggregate and forms a gel. H-70 (hydrogel synthesized at 70 ^{0}C) and H-110 (hydrogel synthesized at 110 ^{0}C) also show the BSA peak but absorb in a broader range from (UV to visible), which makes them a suitable candidate for skin protection from UVB (Figure 3.2 a). H-110 shows a new peak at 340 nm, which suggests that new fluorescent compounds might be generated during the gelation process. H-120 shows the characteristic peak of CQDs at 275 nm due to the π- π* electronic transition of C=C on the CQDs surface. The broad absorbance indicates the presence of a large number of functional moieties present on the surface. Figure 3.3 (b) shows the auto-fluorescence property of various phases of BSA. It is well established that BSA has blue auto-fluorescence because of the aromatic amino acids like tyrosine, tryptophan, and phenylalanine. The emission spectra of H-25 and H-60 show the intrinsic fluorescence like

BSA solution centered at 340-350 nm with the excitation wavelength of 280 nm. The excitation spectrum is also centered at 270-290 nm and does not show long-range excitation.

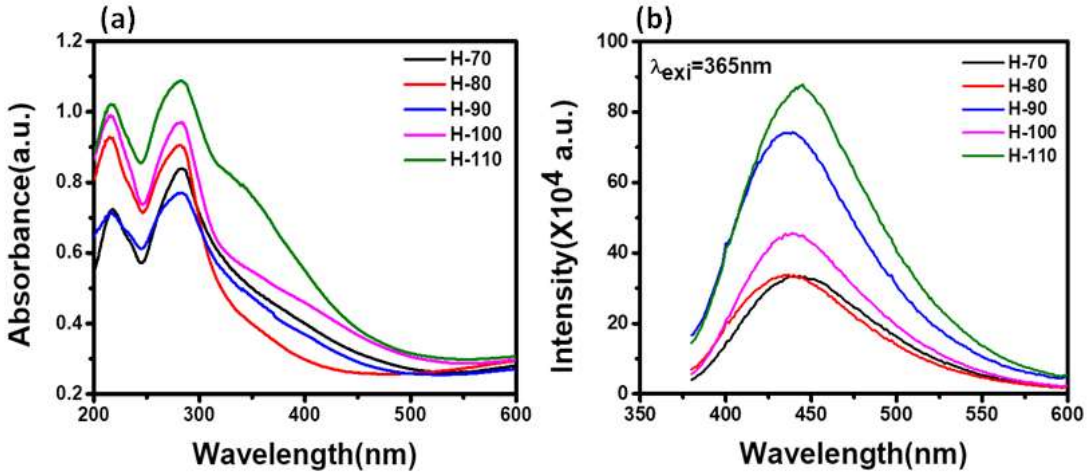

Figure 3.2 (a) Absorbance spectrum of hydrogel phase of BSA protein (H-70 to H-110) (b) Emission spectrum of the hydrogel at an excitation wavelength of 365nm

Moreover, gel phases of the BSA (H-70 to H-110) exhibit strong fluorescence at 450 nm when excited with 365 nm. The PL spectrum of the gels in Figure 3.2 (b) shows a redshift in excitation and emission compared to the sol phase. The emission spectrum ranges from 400-550 nm for emission, with the broad excitation wavelength ranging from 325-375 nm. This phenomenon can be explained by the fact that the heating of the protein reduces the steric hindrance of peptide chains and exposes the aromatic amino acids that can favor the energy transfer among the C=C and C=O bonds that existed in the protein, as well as the proximity of amine groups. Another reason could be the formation of new fluorophores, which have been promoted with the temperature-induced gelation process. The fluorescence intensity increases with the hydrothermal temperature but does not show a strong redshift. Due to a larger number of amino acids and the non-availability of

information regarding their interactions, it isn't easy to probe the exact reason for hydrogels' red-shifted and high auto-fluorescence intensity. The CQDs phase of the BSA shows a blue shift in excitation and emission wavelength compared to the gel phase, which can be tuned by concentration and excitation wavelength. Wavelength-dependent emission in CQDs can be due to the non-uniform size distribution in dispersive medium and various surface functional groups like carboxyl, hydroxyl, and other oxygen species.

FTIR analysis has been performed to get more insight into the involvement of various functional groups in forming different phases of BSA at various temperatures. Full scan FITR spectra (4000-500 cm^{-1}) of all phases of BSA are shown in Figure 3.3 (c). Intensity variation and small spectral shifts have been observed during the gelation process, and some new peaks have been observed when the gel phase is converted to CQDs. The broad peak at 3500 cm^{-1} corresponds to the amide II band due to N-H stretching present in all the phases. From sol to gel transition, only the peak becomes broader, but during the gel to CQDs transition new peak occurs at 3252 cm^{-1}, corresponding to the N-H bond of the amine($-NH_2$) group. Amide band (1400-1700 cm^{-1}) exists during both phase transitions and supports the fact that the main protein chain remains intact after heating at high temperature [174]. Peaks due to amide I bond C=O starch at 1650 cm^{-1} become strong with gel formation but the amide II bond (C-N stretch coupled with N-H bending) at 1580 cm^{-1} disappears in a gel; however, it becomes more robust in the CQD phase. The decrease of amide II at approximately 1580 cm^{-1} and increase of Amide II' at approximately 1450cm^{-1} are related and show the conformational changes at the tertiary structural level. CQDs are nano-dimensional structural with an exposed functional group on the surface. The firm peak around 1400 cm-1 in the CQD phase corresponds to the symmetric stretching vibration of COO^{-}, which disappear in gel form due to CO-NH bond formation and peaks at 1093 cm^{-}

[1] due to C-O vibration becomes prominent in the CQD phase. Due to the limitation of the FTIR instrument, investigation of new chemical bond formation is overruled and limits the accurate analysis of the sol to gel transition.

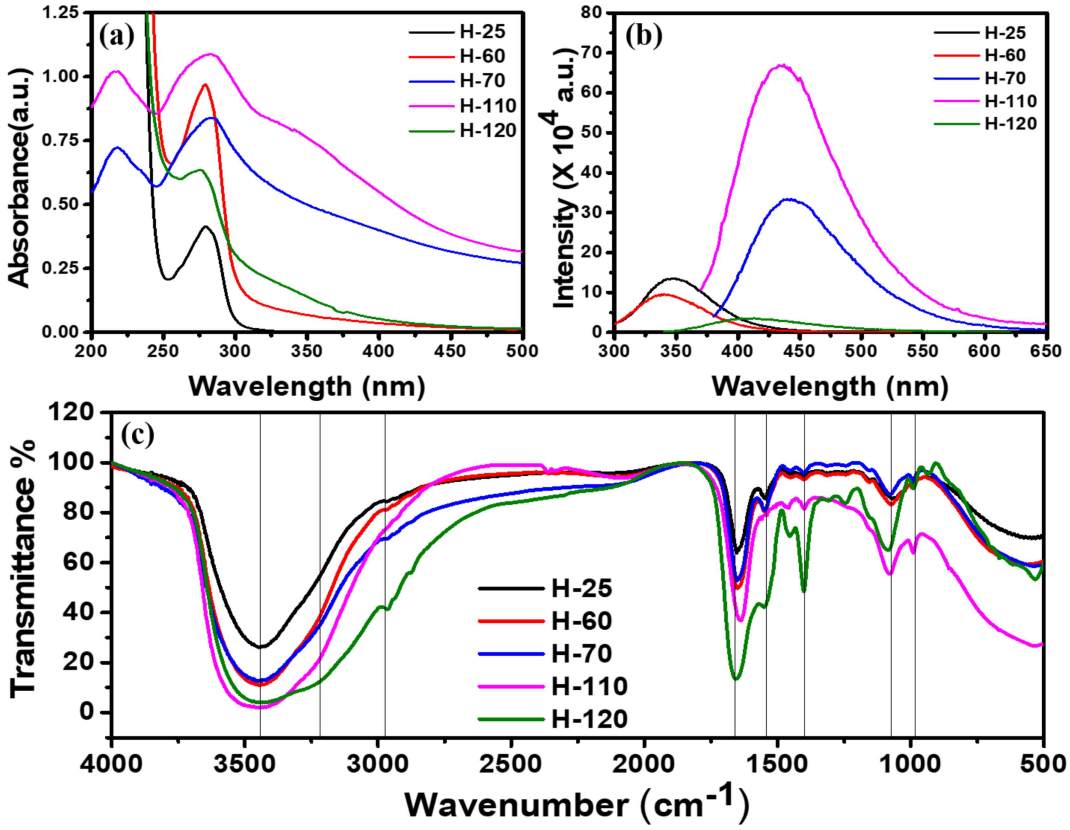

Figure 3.3 (a) UV-Vis spectrum of different phases of BSA protein (b) PL spectrum of different phases of protein at their maximum excitation wavelength (c) FTIR spectrum of different phases

SAXS has been performed on the samples prepared, namely H-25, H-60, H-70, H-90, H-110, and H-120. No gel formation was observed in the samples prepared at temperatures 25 °C and 60 °C and remained in the solution state. On the other hand, gel formation was observed in the samples prepared above the transition temperature. Raw data for the samples are shown in Figure 3.4 (a). Sample H-25 shows a characteristic curve for a sphere. BSA in the solution state was found to form a globular structure, and the radius of the

globule has been calculated by fitting the spherical model. The calculated radius of the BSA is found to be 3.198 nm. Fitted data is shown in Figure 3.4 (b).

For the sample H-60, it is near the phase transition temperature. It was observed that it showed neither the characteristic curve for a sphere nor a gel. As the samples are prepared near the phase transition temperature, it can be assumed that SAXS data will be a combination of both the solution state sample and hydrogels. The mathematical equation used to fit the curve is given by equation (1) [175]:

$$I(q) = \frac{I(0)C}{(1+[(\left(D+\frac{1}{3}\right)(q^2a_1^2)])^{\frac{D}{2}}} + I(0)Gexp^{(-q^2a_2^2)} \qquad \text{-------1}$$

where I(0) is the scaling factor, C is the Lorentz scale, G is the Guinier scale, a_1 is the correlation length, a_2 is related to the radius of gyration of the globule structures of the BSA formed and can be given as $a_2^2 = R_g^2/3$. D is the fractal dimension of the system. The fitted curve for the H-60 is shown in Figure 3.4 (c). Fitted parameters for the H-60 are shown in supplementary Table 3-1.

Table 3-1 Parameters used to fit the equation 1 for the H-60 sample

Lorentz scale (C)	**Guinier scale (G)**	**Radius of gyration (R_g Å)**	**Fractal dimension (D)**	**Correlation length (a1 Å)**
0.75183	5.9978	59.821	1.755	220.39

The value of D indicates the solvent condition. D greater than 2 indicates a bad solvent condition; less than 2 indicates that the BSA is in good solvent condition, and for D value

equal to 2 indicates that BSA is in theta solvent condition. The H-60 sample value of D is 1.75, which is close to 5/3, meaning that the BSA below the transition temperature is in good solvent condition. a_1 Indicates the mesh size of the crosslinks formed. The fitted mess size comes out to be 22 nm. Calculated R_g^2 comes out to be 5.9 nm. From this fitted data, it can be confirmed that BSA molecules start to swell and start to form the network near the transition temperature. The force between the molecules is not strong enough to create a strong network of BSA. Thus, there is a possibility of the existence of both globular structures along with a mesh. For gel samples, namely H-70, H-90, and H-110, fitted data is shown in Figure 3.4 (d). Equation (2) has been used to fit the experimental data below.

$$I(q) = \frac{A}{q^n} + \frac{C}{(1+(q*a_1)^m} \qquad \text{-------2}$$

Where A is the porod constant, C is the Lorentz constant, n is the porod factor, m is the Lorentz factor and a_1 is the mesh size.

The fitting parameters are shown in supplementary Table 3-2. n is the factor that corresponds to the homogeneity of the system. n value above 2 indicates that formed gels are homogeneous. As the temperature increases, the value of n also increases, implying that BSA molecules unfold and form a homogeneous structure with a temperature rise. For H-70, as the temperature is closer to the transition temperature, n is a little less than 2, indicating that the gel structure is not entirely homogeneous and the interaction between the molecules to form the crosslinks is not strong enough. For samples H-90 and H-110, the n value is above 2, and it indicates that samples are homogeneous and bonds are strong enough to form the crosslinks to form stable hydrogels.

Table 3-2 Parameters used to fit the equation-2 for H-70, H-90, and H-110 sample

Parameters	**H-70**	**H-90**	**H-110**
Lorentz scale (C)	85.1	0.07646	0.079
Porod scale (A)	1.3E-04	7.35E-05	7.72E-05
Correlation length (a1 Å)	176.75	19.328	18.3
Porod exponent (n)	1.75	2.3998	2.42
Lorentz exponent (m)	3.26	3.63	3.72

Lorentz part of the curve has two parameters, m and a_1. Lorentz factor m suggests the interaction of the molecules with the solvent. m above the value of 2 indicates that molecules are in poor solvent condition, and the interaction between the molecules is dominating. As the temperature increases, the m value also increases, implying the molecules are coming together to form the denser crosslinks. a_1 value is found to decrease with the increase of temperature, which tells us that distance between the crosslinks is falling. Therefore, this indicates that gels formed at higher temperatures are much denser. Also, for the H-70 sample, as the temperature is near the phase transition, the mess size is larger compared to samples prepared at a higher temperature. This indicates that gels formed are not very dense, and the bonding between the molecules is not strong enough to form thicker gels. For H-120, SAXS scattering is very weak and is very close to the background, so it is not possible to analyze the same.

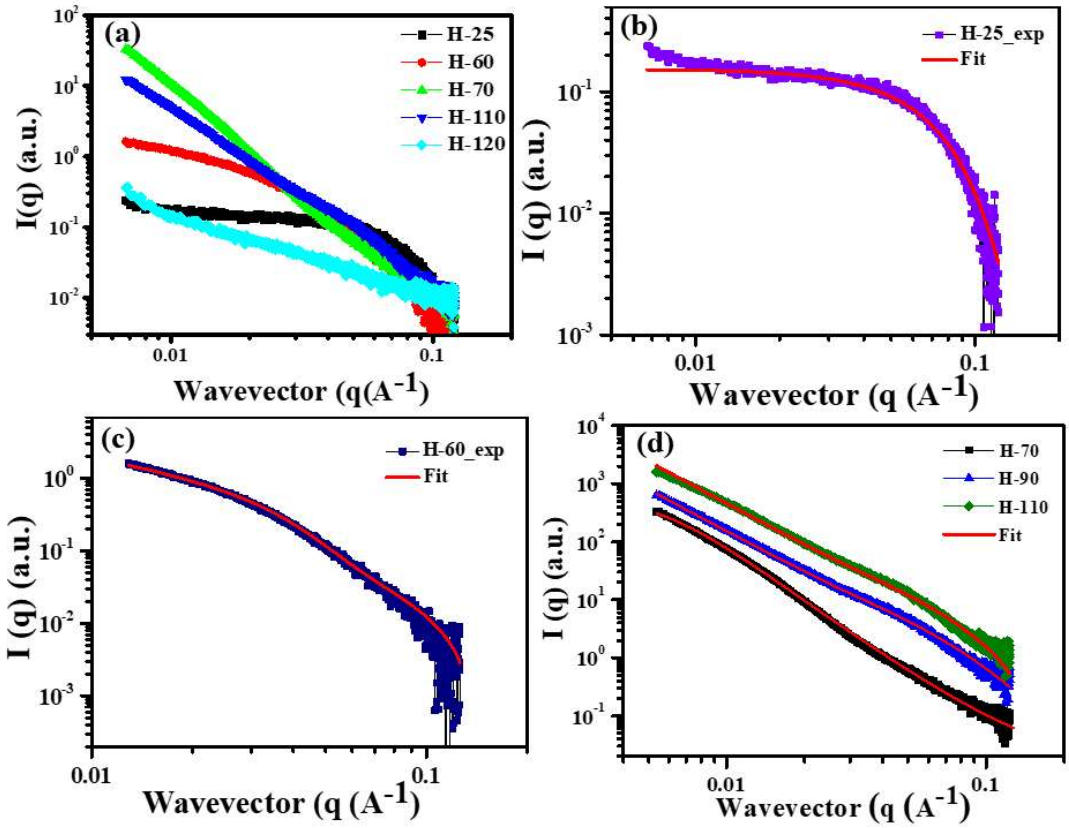

Figure 3.4 (a) Small angle X-ray diffraction analysis of all phases of BSA protein (b) shows that fitting of the SAXS of the H-25 samples using the spherical model (c) H-60 is prepared near the transition temperature, SAXS for H-60 is fitted using the combination of Lorentz and Guinier equation (d) Shows the fitting of H-70, H-90 and H-110 using the Lorentz and Porod fitting.

SEM and rheology studies were employed to investigate the surface morphology and mechanical strength of the temperature elevated self-assembled hydrogels. The SEM images of lyophilized powder of BSA hydrogels (H-70, H-90, H-110) are shown in Figure 3.5 (a), (b), and (c). All hydrogel phases exhibit a three-dimensional, highly porous honeycomb-like structure with irregular shapes and sizes. During the lyophilization process, water evaporates and leaves the voids between the interconnected areas [176]. As there is an increase in the hydrothermal temperature, the pore size of the hydrogels gets smaller. Relative decreases in pore size of hydrogels are shown in Figure 3.5 (d)

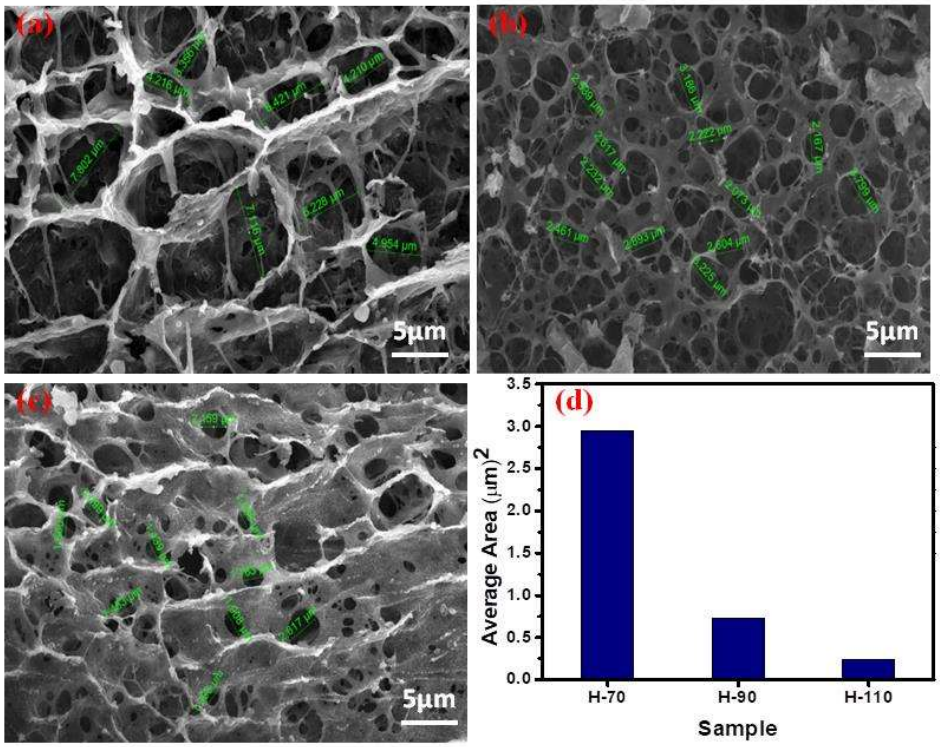

Figure 3.5 SEM images of hydrogel (a) H-70 (b) H-90 (c) H-110 (d) histogram of the area of voids

3.2.3 Rheological analysis

Rheological studies have been performed to investigate the viscoelastic behavior of the hydrogels. Strain sweep test and frequency sweep test were performed to get insight into change in storage and loss modulus of gels as a function of strain and frequency. To evaluate the limits of the viscoelastic region, strain sweep tests were carried out on all the hydrothermally synthesized gel phases of BSA. In the linear viscoelastic area, the storage modulus G′ and viscous modulus G″ are independent of strain and frequency [177]. Under higher strain conditions, the stress response of the gels is no longer sinusoidal, and similarly, higher harmonic contributions lead to a nonlinear stress-strain relationship. In the strain sweep test, G′ and G″ were plotted as a function of strain (%). As we increased the

hydrothermal temperature from 70 ^{0}C to 90 ^{0}C, both G′ and G″ increased linearly shown in Figure 3.6(a). However, at 100 ^{0}C, the G″ and G″ start to decrease, which suggests that due to the hydrothermal process, the lower order structure begins to form that alters the viscoelastic property of hydrogel. Also, for the H-110 phase, we are getting similar viscoelastic trends as H-70. Additionally, in the frequency sweep test, both G′ and G″ moduli also increase as we increase the temperature from 70 ^{0}C to 110 ^{0}C (Figure 3.6 (b)). The higher values of G′ over G″ indicate that the elastic component is predominant on the viscous one in a swiped frequency range.

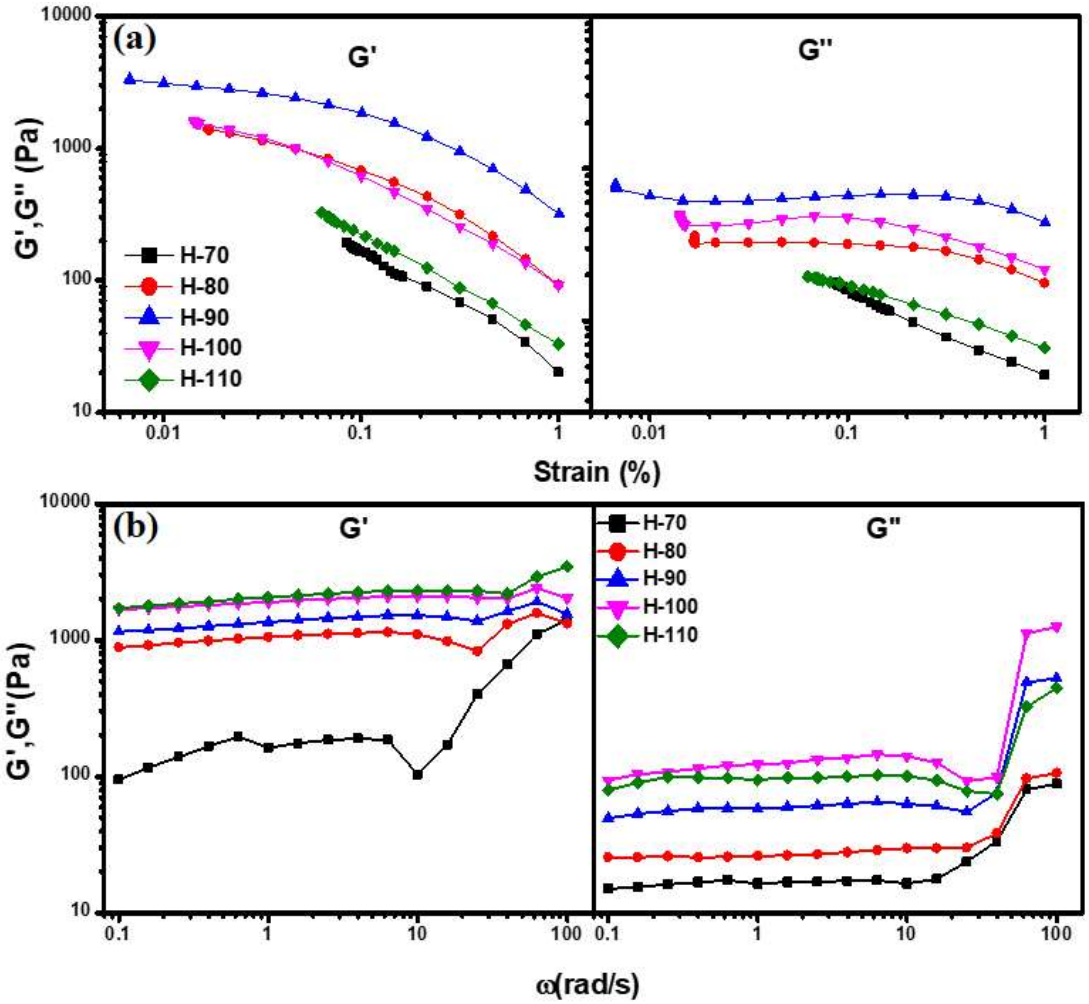

Figure 3.6 (a) Strain sweep test: G′ and G″ modulus as a function of strain (b) frequency sweep test: G′ and G″ modulus as a function of frequency.

3.2.4 Cell toxicity and cellular uptake analysis

Bovine serum albumin (BSA) has been extensively used in biomedical applications due to its higher bioavailability, biocompatibility, and biodegradability properties [178]. Our objective was to study the cytotoxicity aspect of synthesized BSA hydrogel using BSA at various temperatures. *In vitro*, the biocompatibility of all hydrogel samples, i.e., H-25, H-60, H-70, H-80, H-90, H-100, H-110, H-120, and H-200, were studied and shown in Figure 3.7. MTT assay results demonstrated that all samples showed % cell survival from 93.6% to 99.16%, suggesting its excellent biocompatibility. Among them, H-110 showed the highest % cell survival of 99.16 %.

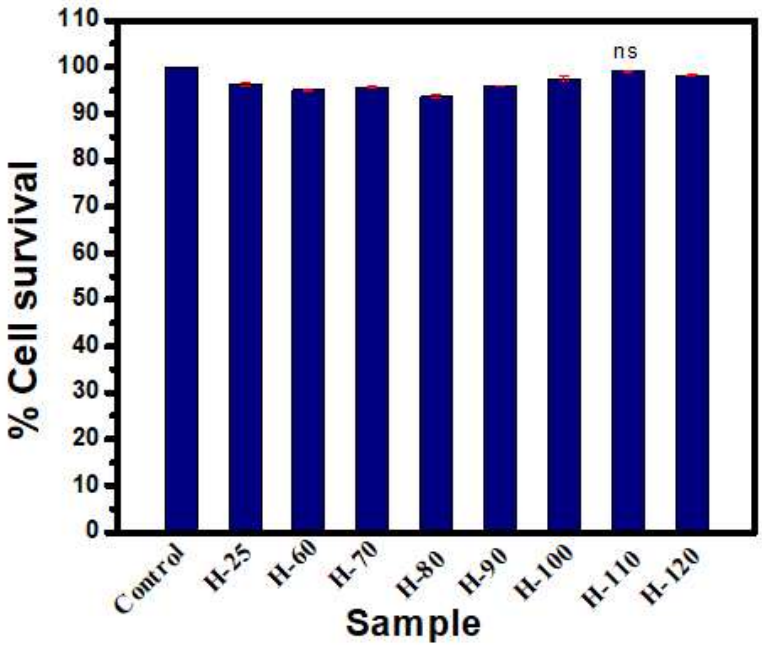

Figure 3.7 Cell viability study of hydrogel samples for 24 h. Vertical bars representing (mean ± SEM). Significance was tested using one-way ANOVA followed by the Tukey Post-hoc test.

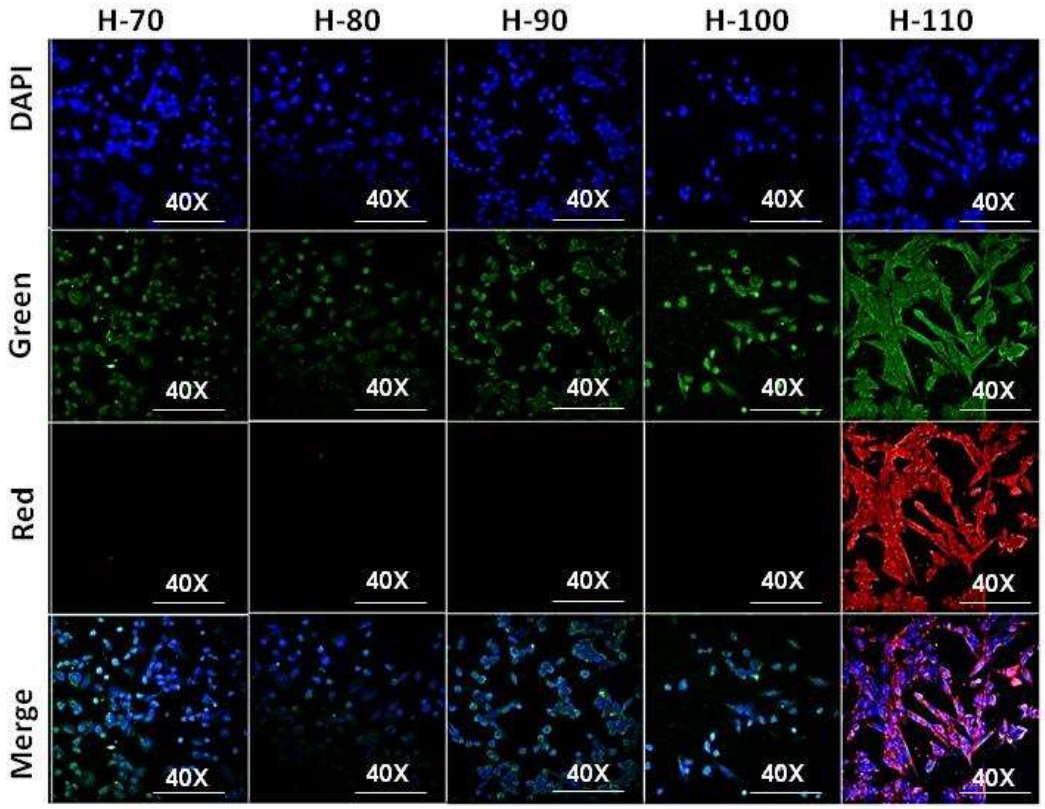

Figure 3.8 Confocal imaging of cellular uptake of H-60, H-70, H-80, H-90, H-100 and H-110

Cellular uptake studies confirm its good bioimaging green autofluorescence capacity in all hydrogel samples. Interestingly, H-110 has shown maximum cellular penetration (Figure 3.8) with a higher cytoplasmic and nuclear distribution. Hence, we have applied H-110 for further experimental studies.

3.2.5 Studying the protective role of H-110 on UVB induced cytological damaged primary skin cells

UVB attenuation activity of all the samples was tested and shown in Figure 3.9. All the gel phases have shown a significant reduction in UVB intensity. However, maximum attenuation is shown by H-110 with a density of 5 mg/cm^2. The maximum UVB irradiance

emitted by the UVB source was 790 μW/cm ^{2} at 11 cm away from the center of the rod, where all the UVB attenuation studies were performed. The exact amount of hydrogels was cut and loaded at the same place to reduce the effect of variable parameters in UVB attenuation. The maximum attenuation is observed by H-110 hydrogel with a 36.7 % decrease.

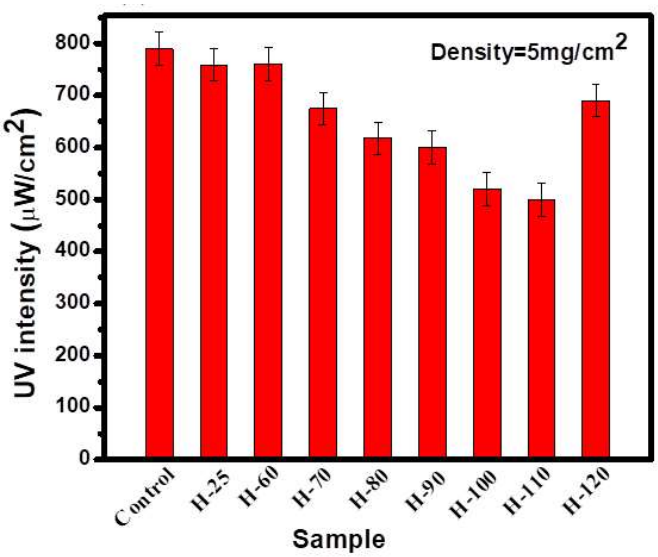

Figure 3.9 UVB attenuation using different phases of BSA hydrogels

Our MTT data has demonstrated aggressive normal skin cell death except UVB treated cells after all three-time points, i.e., 5 min, 10 min, and 15 min (P<0.000, One-Way ANOVA, followed by Tukey Posthoc test. Minimum % cell survival was observed after 15 min UVB treatment (29.39 %) in comparison to control skin cells (P<0.000, One-Way ANOVA, followed by Tukey Posthoc test). No significant cell death was observed after 5 min UVB exposure in H-110 applied skin cells compared to control skin cells (P=0.997, One-Way ANOVA, followed by Tukey Posthoc test). After 20 and 15 min of UVB exposure, the H-110 applied cells showed 84.06 % and 77.76 % cell survival. Interestingly,

the H-110 layer on skin cells significantly increased skin cell survival at 47.33 %, 39.09 %, and 50.36 % after 5 min, 10 min, and 15 min UVB exposure, respectively (Figure 3.10) (P<0.000, One-Way ANOVA, followed by Tukey Posthoc test) [179].

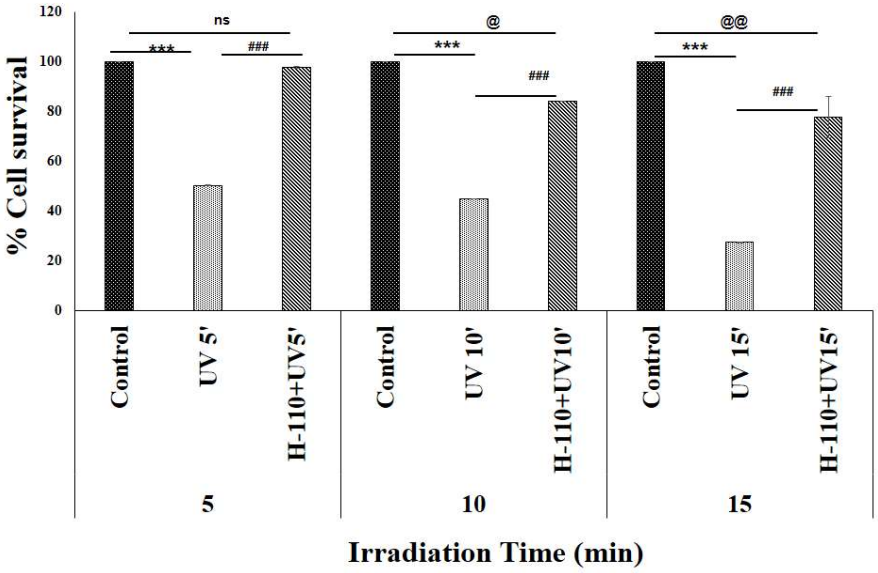

Figure 3.10 Protective role of H-110 from UVB induced cytological damage primary skin cell culture by % cell viability assay, time dependent experimental settings (5-15 min). Vertical bars representing (mean ± SEM). Significance was tested using one-way ANOVA followed by Tukey Post-hoc test. *showed the significance level between control and only UVB, # showed the significance level between only UVB and H-110+UVB and @ showed the significance level between only control and H-110+UVB. Data was considered statistically significant as ***/###/@@@ for P<0.0001, **/##/@@ for P<0.01 and */#/@ for P<0.05.

It was observed that the confocal imaging data (Figure 3.11) is also in accordance with the results of the MTT assay with the protective role of H-110 after UVB treatment. In our study, with an increase of UVB exposure time to cells from 5 min to 15 min, the intensity of emitted red fluorescence decreases. This might be due to the disruption of cellular components with increased time of UVB exposure as the morphology of cells was also changed towards dead cells at 15 min UVB exposed group. Previous studies have reported that the cell partially absorbs the smaller UV wavelength and emits a longer wavelength.

However, in the case of the H-110 in applied group of cells, no significant morphological changes were observed after UVB exposure. Hence, this clearly shows that H-110 has the potential to protect the skin cells from UVB exposure.

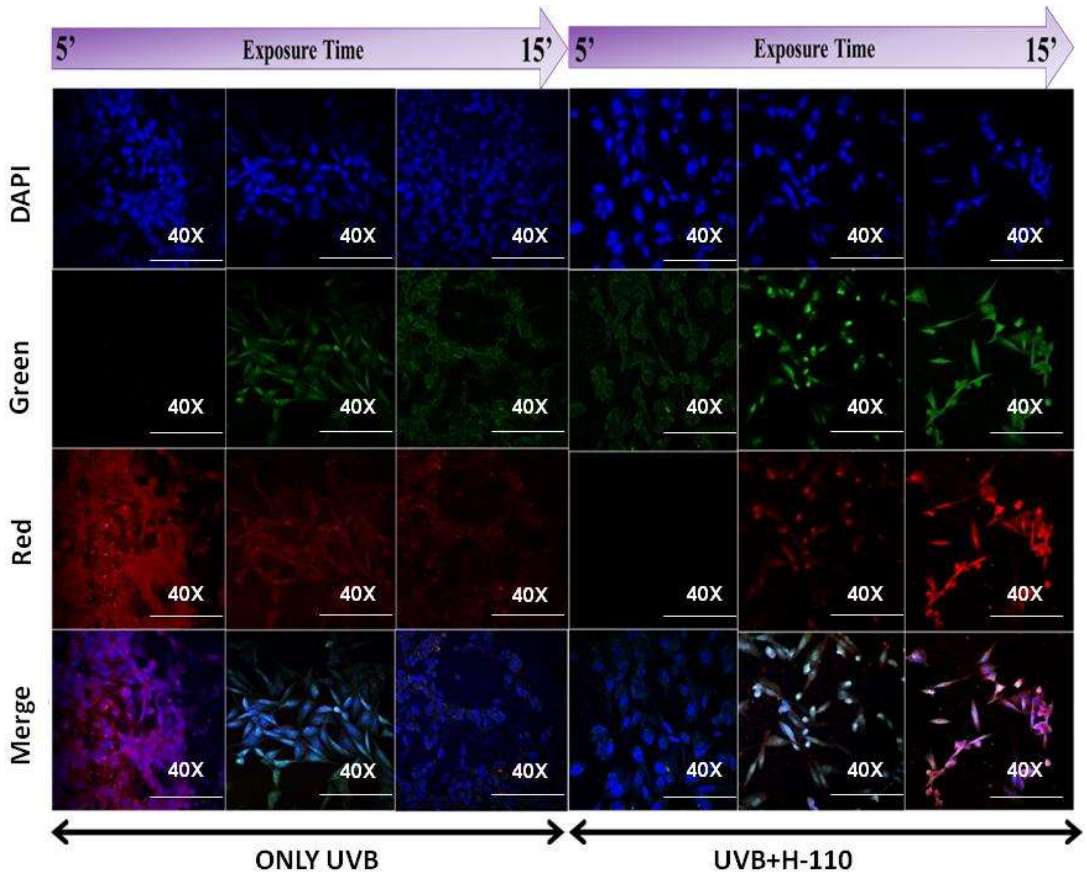

Figure 3.11 Protective role of H-110 from UVB induced cytological damage primary skin cell culture by confocal bioimaging, time-dependent experimental settings (5-15 min).

3.2.6 *In vivo* protective role of H-110 on UVB induced skin damage in mice

Our histological results with 3 days of UVB exposure (Figure 3.12 (b)) showed no significant change, whereas 5 days of UVB exposure (Figure 3.12 (c)) produced pathomorphological changes in the skin of mice, i.e., considerable thickening of stratum

corneum (SC) and epidermis (Tep, P<0.000) and perivascular edema (Ed) in the dermis was prominent. At H-110 monolayer applied group showed no significant morphometric changes after 3 days of UVB exposure (Figure 3.12 (d)). Interestingly, 5 days of UVB exposure at the H-110 monolayer (Figure 3.12 (f)) applied group showed significant epidermal thickening as compared to control tissues (P<0.007).

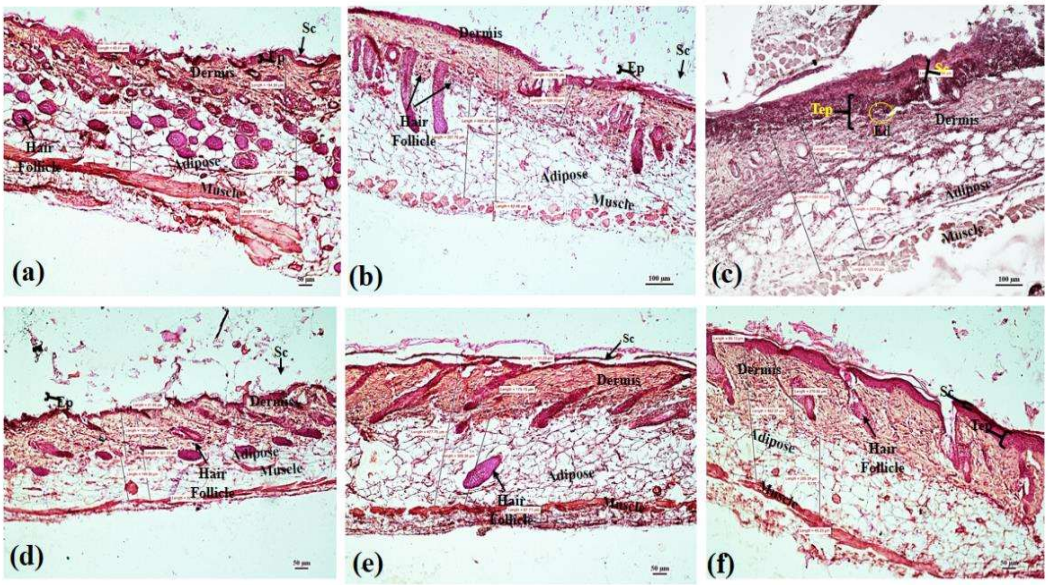

Figure 3.12 Histoarchitecture of skin tissue. (a) Control, (b) UVB treated for 3 days, (c) UVB treated for 5 days, (d) H-110 treated, (e) H-110+UV treated for 3 days and (f) H-110+UV treated for 5 days.

However, when the epidermal thickness of H110+UV5D skin tissues was compared with the epidermal thickness of the UV5D skin tissue, the epiderma was significantly thinner in H-110+UV5D skin tissue (P<0.000, Figure 3.13). Hence, our mice model study also supports our finding that topical administration of H-110 is potentially effective in protecting skin from UVB-induced skin damage. Ep represents epidermis, Sc represents stratum corneum, Tep represents thickening epidermis, and Ed represents edema.

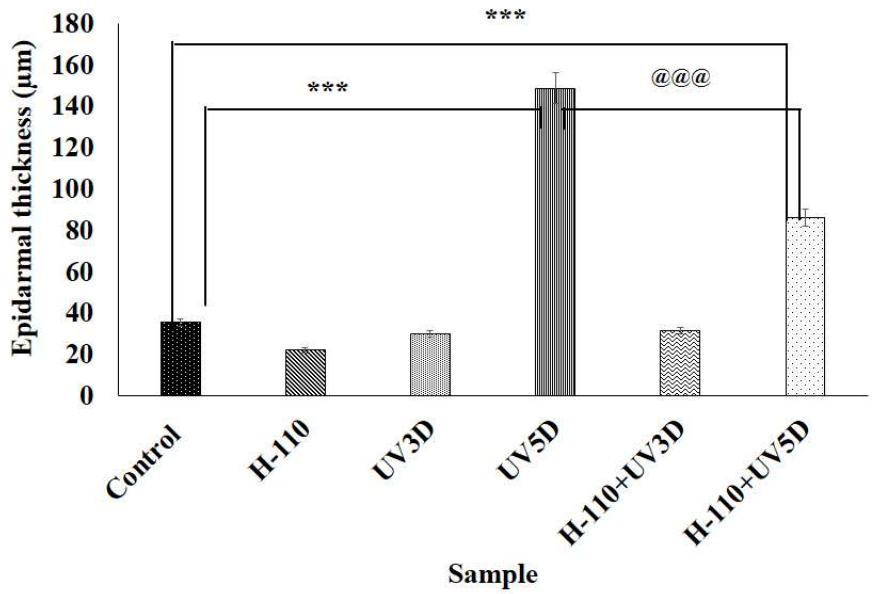

Figure 3.13 Epidermal thickness of different treatment groups, Vertical bar representing epidermal thickness of different treatment groups (mean ± SEM). Significance was tested using one-way ANOVA followed by Tukey Post-hoc test. *showed the significance level between control and only UVB 5 days, # showed the significance level between control and H-110+UVB 5 days and @ showed the significance level between only UVB 5 days and H-110+UVB 5 days. Data were considered statistically significant as ***/###/@@@ for $P<0.0001$.

3.3 Conclusion

Using a simple and efficient hydrothermal method, a wide range of phases varying from sol-gel-sol of BSA was synthesized. This is the first-of-this-kind of study wherein we observed that even without using cross-linkers, we could synthesize different phases of protein by varying the hydrothermal temperature. Extensive physico-chemical and optical characterization data of synthesized hydrogels have shown potential application as a UVB blocker for skin protection. Cytotoxicity and UV protection ability of hydrogels were tested using primary skin cells. Among all, the H-110 sample has shown extraordinary applicability. Thus, *in vivo* protective role of H-110 on UVB-induced skin damage in the

mice model was studied. Results have confirmed that topical administration of H-110 potentially effective in protecting skin from UVB-induced skin damage. The present study ensures that by using BSA protein as a precursor, it is possible to prepare hydrogels with various functionalities and no cytotoxicity and holds a prominent role in the biomedical field for the protection of skin and the cure of skin cancer.